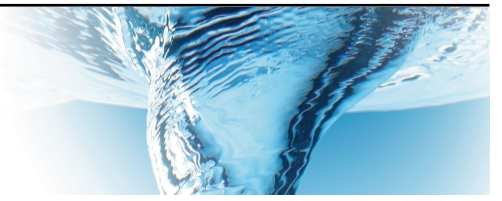
J. Fluid Mech. (2026), *vol.* 1043, R4, doi:10.1017/jfm.2026.12017



An iterative method to link surface roughness and turbulent mean-flow response using resolvent analysis

Miles Chan[1], **Oliver Khan**[2], **Ugo Piomelli**[3] **and Beverley McKeon**[2]

[1]Graduate Aerospace Laboratories, California Institute of Technology, Pasadena, CA 91125, USA

[2]Center for Turbulence Research, Stanford University, Stanford, CA 94305, USA

[3]Department of Mechanical and Materials Engineering, Smith Engineering, Queen's University, Kingston, ON K7L 3N6, Canada

Corresponding author: Beverley McKeon, bjmckeon@stanford.edu

(Received 25 March 2026 UTC; revised 5 June 2026 UTC; accepted 26 June 2026 UTC)

A physics-based model is developed to predict the spatially varying sensitivity of turbulence to roughness geometry and the corresponding flow modifications. Resolvent analysis with a drag-normalized, Reynolds-decomposed volume penalization is formulated to efficiently link the mean flow profile to predictions of the drag force, wake field fluctuations, and dispersive stresses for broadband (sandgrain) surface roughness. An eddy viscosity approach models the modification of the stochastic stress arising due to the attenuation of convecting fluctuations within the roughness sublayer. Crucially, these components link the mean-flow profile to the force profiles and stresses which determine its shape, so that the model can be iteratively solved for a given bulk flow over a surface roughness, starting from an initial corresponding smooth wall flow condition. For engineering-relevant surface geometries in flows which respect outer similarity, the model output estimates turbulent-drag response, namely equivalent sandgrain roughness, Hama roughness-function and spatial variation of roughness sublayer (wake field) turbulent fluctuations. The approach is demonstrated on a channel flow with sandgrain roughness at an engineering-relevant Reynolds number.

Key words: turbulent boundary layers

© The Author(s), 2026. Published by Cambridge University Press. This is an Open Access article, distributed under the terms of the Creative Commons Attribution licence (https://creativecommons.org/licenses/by/4.0/), which permits unrestricted re-use, distribution and reproduction, provided the original article is properly cited.

https://doi.org/10.1017/jfm.2026.12017 Published online by Cambridge University Press

1. Prediction of turbulent flow characteristics over rough walls

Predicting roughness effects on near-wall turbulence remains a topic of paramount practical importance, since most engineering-relevant flows are turbulent, most surfaces are not hydrodynamically smooth, and the influence of roughness on engineering quantities (e.g. drag) may be significant. Despite sustained interest in the topic, many methods of quantifying the effects of roughness on wall turbulence remain at least semiempirical, relating predominantly to global statistics of the roughness geometry. In this work, we provide a framework by which to understand flow sensitivity and turbulent response to specific scales of roughness, the development of dispersive stresses and their feedback on the mean velocity (figure 1*a*). The end result is the iterative loop relating a scan of roughness geometry to the associated mean flow response shown in figure 1(*b*) (Chan 2024).

In many complex, high-Reynolds-number engineering-relevant flows with flow over fully developed rough walls, the representative geometric roughness scale, for example the sandgrain roughness height, k, is small with relation to the outer flow scale, δ. Besides an increase in the drag at the wall due to the presence of the roughness, and therefore an increase in the friction velocity, u_τ, the direct effect of roughness in this regime is generally confined to the roughness sublayer, a region which extends from the wall $y = 0$ to $y \approx (3-5)k$. By Townsend's hypothesis, flow outside of the roughness sublayer reflects the changed u_τ, but otherwise retains the similarity characteristics of a smooth wall at the same friction Reynolds number, $Re_\tau = \delta^+ = \delta u_\tau/\nu$, where ν is the kinematic viscosity. The global effects of roughness on the mean velocity field and drag are encapsulated by the equivalent sandgrain roughness k_s^+ and Hama roughness-function ΔU^+, which are fundamentally due to the spatially varying modulation of the near-wall turbulence by the surface roughness and the introduction of drag forces on the roughness elements.

Many efforts to model turbulence over realistic, multiscale surface geometries bypass the details of the spatially varying roughness sublayer fluctuations and focus instead on directly predicting k_s^+ and/or ΔU^+ given averaged statistics and spectral information about the roughness using empirical models. The literature is broad and has been recently reviewed by Flack & Chung (2022). One especially effective physics-based effort is the wind-shade model of Meneveau *et al.* (2024) which uses minimal empirical assumptions to link surface features of realistic roughness to the resulting drag. In a paper of direct relevance to the present work, Mejia-Alvarez & Christensen (2010) demonstrated that low-order representations of roughness on a wind turbine surface produced similar stresses to the full surface geometry, indicating that only certain geometric scales contribute to the drag response or, equivalently, that the flow sensitivity is roughness-scale-dependent. It remains desirable to seek model forms that more directly encode the physics linking roughness features to the drag response through modelling the roughness sublayer fluctuations and their spatially varying effects.

Here we introduce resolvent analysis with volume penalization (RAVP). The efficacy of the RAVP modelling framework is tested using the direct numerical simulation (DNS) of a channel flow over sandgrain roughness in the fully rough regime conducted by Hantsis & Piomelli (2020). Full details of the solution, which uses a second-order accurate central difference in space on a staggered mesh and a second-order accurate semi-implicit time advancement method may be found therein; we summarize the simulation conditions in table 1. Sandgrain roughness consisting of randomly oriented ellipsoids with semiaxes k, $1.4k$ and $2k$, where $k = 0.04\delta$, is modelled symmetrically on both walls using the immersed boundary method (IBM). In the fully rough regime, $k_s \approx 1.6k$ for this geometry. The simulation is run at a constant $Re_b = 21\,400$ and temporal averages are computed over 50 eddy turnover times.

https://doi.org/10.1017/jfm.2026.12017 Published online by Cambridge University Press

	Re_τ	u_τ/U_b	ΔU^+	k_s^+	k/δ	L_x/δ	L_y/δ	L_z/δ	N_x	N_y	N_z	Δx^+	Δy^+_{min}	Δz^+
DNS	1745	0.0814	9.2	112	0.04	6	2.064	3	1024	530	512	10.2	0.84	10.2
RAVP-M	1739	0.0813	9.3	114	—	—	—	—	—	—	—	—	—	—

Table 1. Numerical domain (L_x, L_y, L_z) and simulation parameters (top line) and RAVP-M predictions after $N_{eval} = 162$ iterations through the loop of figure 1(*b*).

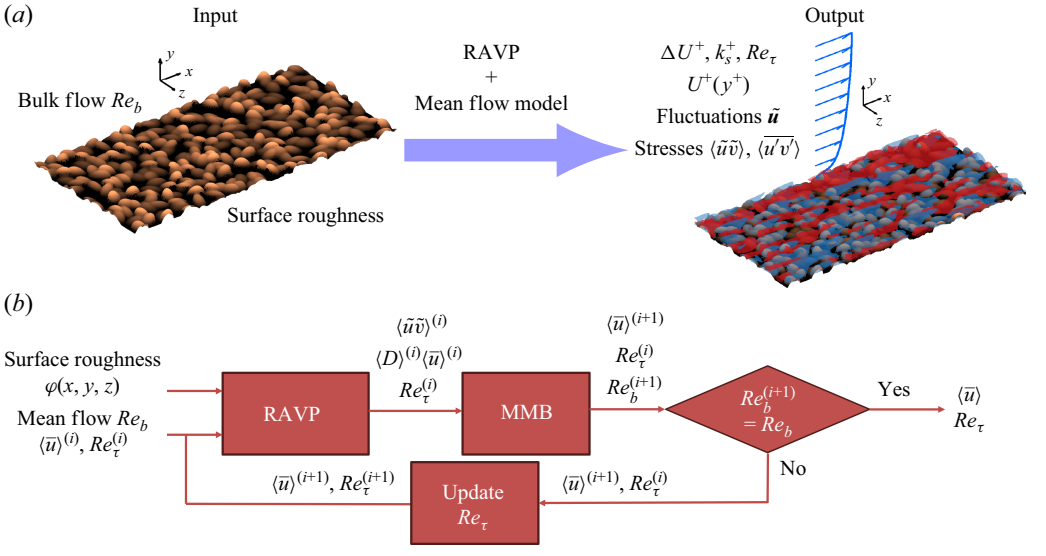


Figure 1. (*a*) An input–output framework relating surface-specific roughness geometry input at a given flow condition, here specified by bulk Reynolds number, Re_b, to the corresponding global (averaged) and local (spatially varying) flow features using RAVP and a mean flow model. (*b*) Iterative loop of RAVP coupled to the mean momentum balance (MMB) to recover the mean velocity profile, which we identify as RAVP-M.

2. A drag-scaled, Re-decomposed volume penalization in resolvent analysis

Resolvent analysis provides a method to predict the modal structure that is most amplified by the Navier–Stokes operator linearized relative to the mean field. The method has been extensively documented in the literature, e.g. McKeon (2017), thus we describe here the modified RAVP. We use RAVP to obtain a transfer function relating velocity response in the form of modes describing the wake field, or the zero frequency variations from the spatially averaged velocity fields, to roughness geometry, given a mean flow profile and a surface scan of an engineering-relevant roughness. We note that other authors have considered related resolvent-based approaches of non-spatially uniform boundary conditions, including rough walls that can be well described by a single wavenumber and its harmonics via the solution of wavenumber-coupled resolvent systems. In particular, for riblet surfaces Chavarin & Luhar (2020) developed a volume penalization method using a permeability function to drive the flow velocity to zero in the solid region and Flynn *et al.* (2024) developed a projection-based immersed boundary method and applied it to a sinusoidal roughness.

We consider the continuity equation and the momentum equations for incompressible turbulent channel flow of a Newtonian fluid augmented by a forcing term that accounts for

https://doi.org/10.1017/jfm.2026.12017 Published online by Cambridge University Press

the presence of the roughness, $-\boldsymbol{F}^{RA}$:

$$\frac{\partial \boldsymbol{u}}{\partial t} + \boldsymbol{u} \cdot \boldsymbol{\nabla} \boldsymbol{u} = -\boldsymbol{\nabla} p + \frac{1}{Re_\tau} \nabla^2 \boldsymbol{u} - \boldsymbol{F}^{RA}, \qquad \boldsymbol{\nabla} \cdot \boldsymbol{u} = 0. \tag{2.1}$$

A triple decomposition is used to identify the intrinsic spatiotemporal average, $\langle \overline{q} \rangle(y)$, the wake field, $\tilde{q}(x, y, z)$, and the spatially and temporally varying component, $q'(x, y, z, t)$,

$$q(x, y, z, t) = \langle \overline{q} \rangle(y) + \tilde{q}(x, y, z) + q'(x, y, z, t). \tag{2.2}$$

For flow quantities, the intrinsic average $\langle \cdot \rangle$ is calculated at each xz-plane as the average of the quantity over the fluid-occupied area, and is used in the triple decomposition to define the wake field. The area fraction occupied by fluid is denoted $\Phi(y)$, and is calculated as the plane average of the volume of fluid fraction (VOF) $\varphi(x, y, z)$. The superficial average $\langle \cdot \rangle_s$ is calculated by summing the quantity over the fluid-occupied area and dividing by the full plane area, and is related to the intrinsic average by $\langle \cdot \rangle_s = \Phi \langle \cdot \rangle$. We use a strict VOF representation, where any cell with $\varphi < 1$ is set to $\varphi = 0$, such that when a spatial (plane) average is taken over a fluid quantity, denoted by $\langle \cdot \rangle_{xz}$, multiplied by φ, only data in cells which do not contain any of the solid are considered (effectively a low-pass spatial filter). The plane average $\langle \cdot \rangle_{xz}$ is calculated as the sum of a quantity over the full plane area, divided by the full plane area. The plane and superficial averages are equal when the quantity is equal to zero within the fully roughness-occupied area.

The (spatially varying) force, $\boldsymbol{F}^{RA}$, reflects the roughness geometry, and is of the same form as the IBM forcing, i.e.

$$F_i^{RA}(x, y, z) = Du_i = [1 - \varphi(x, y, z)] D_{max} u_i, \;\; F_i^{IBM}(x, y, z) = -[1 - \varphi(x, y, z)] \frac{1}{\Delta t^n} u_i. \tag{2.3}$$

Here subscript i and Δt^n denote the ith component and nth time step, respectively. Here F_i^{RA} depends on the roughness geometry expressed in terms of the VOF and a real-valued magnitude parameter D_{max}, which is closed to normalize the integral of the drag term using the mean streamwise momentum equation computed by plane averaging,

$$\frac{1}{Re_\tau} \frac{\mathrm{d} \langle \overline{u} \rangle_s}{\mathrm{d}y} - \langle \overline{u'v'} \rangle_s - \langle \tilde{u}\tilde{v} \rangle_s + \int_y^1 \langle D\overline{u} \rangle_{xz} \, \mathrm{d}y' = 1 - y, \tag{2.4}$$

$$\int_0^1 \langle D\overline{u} \rangle_{xz} \, \mathrm{d}y' = D_{max} \int_0^1 \left[\langle 1 - \varphi \rangle_{xz} \langle \overline{u} \rangle_s - \langle \tilde{\varphi}\tilde{u} \rangle_{xz} \right] \mathrm{d}y' = 1. \tag{2.5}$$

The time average (indicated here by an overline), stochastic fluctuations and $\tilde{v}$ have zero value in the roughness sublayer for a channel flow. Thus, plane averages and superficial averages are equivalent for the temporally averaged $\overline{u}$, the stochastic stress $\overline{u'v'}$ and the dispersive stress $\tilde{u}\tilde{v}$. Assuming that $\langle \tilde{\varphi}\tilde{u} \rangle_{xz}$ is small (since it is the product of two spatial variations), a scalar D_{max} can be determined. Or, utilizing the form of the IBM force in the simulation, which corrects the velocity to zero inside of the roughness, a wall-normally varying function $\mathcal{D}_{max}(y)$ which matches the equivalent IBM force profile $\langle \overline{F_1^{IBM}} \rangle_{xz}$, may also be determined for comparison with the scalar D_{max},

https://doi.org/10.1017/jfm.2026.12017 Published online by Cambridge University Press

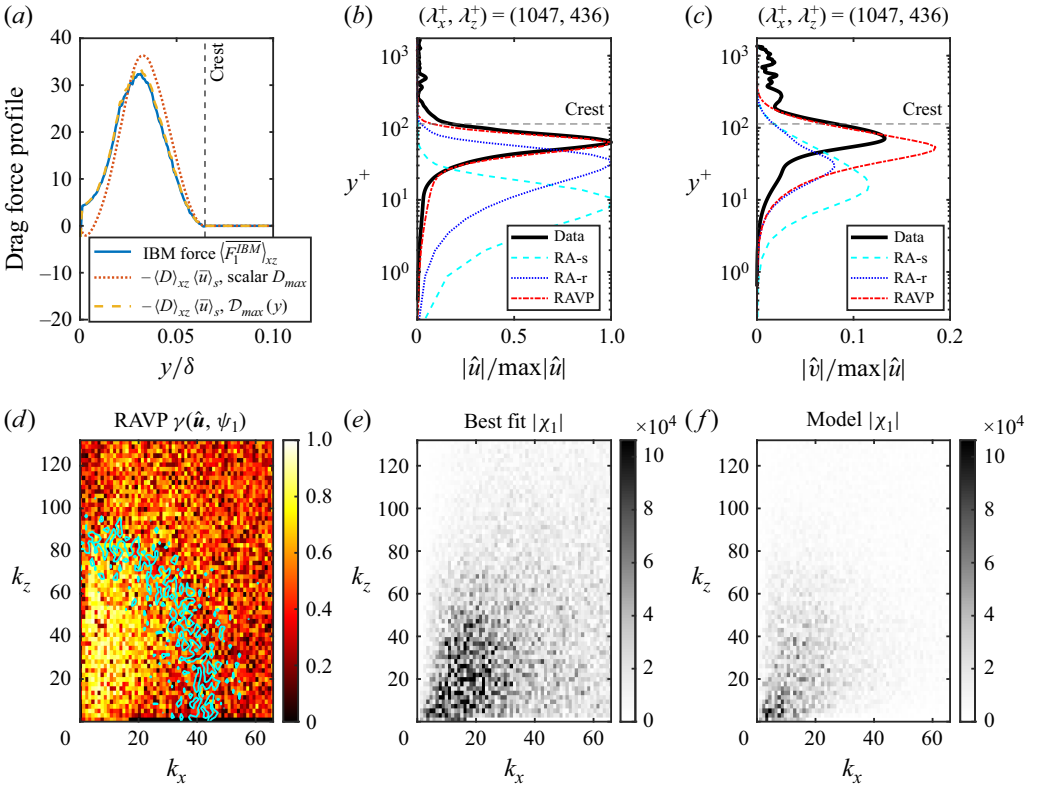


Figure 2. (*a*) Forcing in (2.1): RAVP with a scalar D_{max} shows good agreement with the plane-averaged drag term from the IBM simulation (data) and RAVP with $\mathcal{D}_{max}(y)$ tuned to match the IBM force. (*b,c*) RAVP improves the agreement between the shape of the first resolvent response modes and DNS wake field modes (data) relative to traditional resolvent analysis using smooth wall (RA-s) and true rough wall (RA-r) mean profiles for u and v, respectively, from a sample mode with $(\lambda_x^+, \lambda_z^+) = (1047, 436)$. (*d*) Spectrum of the projection coefficient for the wake field data onto the first symmetric RAVP mode. The overlaid contour indicates where the wake field turbulent kinetic energy (TKE) is 10 % of its maximum. (*e*) Spectrum of the weights $\chi_{\boldsymbol{k},1}$ computed from (2.8) which includes all forcing inputs to the resolvent operator. (*f*) Spectrum of the weights $\chi_{\boldsymbol{k},1}$ for the compressed model computed using (2.9) which only includes the linear forcing term $-\hat{D}_{\boldsymbol{k}} \langle \overline{\boldsymbol{u}} \rangle_s$.

$$D_{max} = \frac{1}{\int_0^1 \langle 1 - \varphi \rangle_{xz} \langle \overline{u} \rangle_s \, \mathrm{d}y'}, \qquad \mathcal{D}_{max}(y) = -\frac{\langle \overline{F_1^{IBM}} \rangle_{xz}}{\langle 1 - \varphi \rangle_{xz} \langle \overline{u} \rangle_s}. \tag{2.6}$$

Both drag models provide reasonable agreement with the true IBM force (figure 2*a*), however, the scalar D_{max} may be used without having completed an IBM simulation. Under these assumptions, the drag force profile is approximated as $\langle D\overline{u} \rangle_{xz} \approx \langle D \rangle_{xz} \langle \overline{u} \rangle_s$.

By Reynolds decomposing the volume penalized drag term as well as the turbulent state relative to the plane average, and denoting the Fourier-transformed state at a given streamwise wavenumber, spanwise wavenumber and temporal frequency triplet, $\boldsymbol{k} = (k_x, k_z, \omega)$, by $\hat{\cdot}$, we obtain an expression for the modified resolvent operator,

$$\begin{bmatrix} \hat{\boldsymbol{u}}_{\boldsymbol{k}} \\ \hat{p}_{\boldsymbol{k}} \end{bmatrix} = \left(-i\omega \begin{bmatrix} \boldsymbol{I} & 0 \end{bmatrix} - \begin{bmatrix} \mathcal{L}_{\boldsymbol{k}} - diag\,\langle D \rangle_{xz} & -\boldsymbol{\nabla} \\ \boldsymbol{\nabla}^\top & 0 \end{bmatrix} \right)^{-1} \left(\hat{\boldsymbol{f}}_{\boldsymbol{k}} - \hat{D}_{\boldsymbol{k}} \langle \overline{\boldsymbol{u}} \rangle_s + \hat{\boldsymbol{d}}_{\boldsymbol{k}} \right). \tag{2.7}$$

https://doi.org/10.1017/jfm.2026.12017 Published online by Cambridge University Press

Here $\mathcal{L}_k$ is the usual linearized Navier–Stokes operator (linearized relative to the superficial mean velocity), $\boldsymbol{\nabla}$ is the gradient, N_y is the number of discretization points in the wall-normal direction, and zero mean wake velocities, $\langle\overline{v}\rangle_s$ and $\langle\overline{w}\rangle_s$, are assumed. Standard channel flow boundary conditions are used here, i.e. the boundary conditions are not modified by the roughness geometry. Relative to the classical, smooth wall analysis, the resolvent is modified directly by the plane-averaged drag force, $diag\,\langle D\rangle_{xz}$. With $\boldsymbol{u}'' = \tilde{\boldsymbol{u}} + \boldsymbol{u}'$, two additional forcing terms beyond the usual nonlinear interaction of velocity fluctuations $\hat{\boldsymbol{f}}_{\boldsymbol{k}} = -(\boldsymbol{u}''\cdot\boldsymbol{\nabla}\boldsymbol{u}'' - \langle\overline{\boldsymbol{u}''\cdot\boldsymbol{\nabla}\boldsymbol{u}''}\rangle_{xz})_{\boldsymbol{k}}$ represent (i) the coupling between the roughness and the superficial mean flow ($\hat{D}_{\boldsymbol{k}}\,\langle\overline{\boldsymbol{u}}\rangle_s$) and (ii) nonlinear interactions between the spatially varying $\hat{D}_{\boldsymbol{k}}$ and spatially and temporally varying velocity modes, $\hat{\boldsymbol{d}}_{\boldsymbol{k}} = -(\tilde{D}\boldsymbol{u}'' - \langle\tilde{D}\tilde{u}\rangle_{xz})_{\boldsymbol{k}}$. The full state may be expanded in the usual way in terms of a weighted singular value decomposition of the resolvent, $\mathcal{H}_{\boldsymbol{k}} = \sum_{j=1}^{N}\sigma_{\boldsymbol{k},j}\psi_{\boldsymbol{k},j}\phi_{\boldsymbol{k},j}^{\dagger}$, i.e.

$$\begin{bmatrix}\hat{\boldsymbol{u}}_{\boldsymbol{k}}\\ \hat{p}_{\boldsymbol{k}}\end{bmatrix} = \mathcal{H}_{\boldsymbol{k}}\left(\hat{\boldsymbol{f}}_{\boldsymbol{k}} - \hat{D}_{\boldsymbol{k}}\,\langle\overline{\boldsymbol{u}}\rangle_s + \hat{\boldsymbol{d}}_{\boldsymbol{k}}\right) = \sum_{j=1}^{N}\sigma_{\boldsymbol{k},j}\psi_{\boldsymbol{k},j}\chi_{\boldsymbol{k},j} \quad \text{with} \quad \chi_{\boldsymbol{k},j} = \left\langle\phi_{\boldsymbol{k},j}, \hat{\boldsymbol{f}}_{\boldsymbol{k}} - \hat{D}_{\boldsymbol{k}}\langle\overline{\boldsymbol{u}}\rangle_s + \hat{\boldsymbol{d}}_{\boldsymbol{k}}\right\rangle. \tag{2.8}$$

Here $\hat{D}_{\boldsymbol{k}}\,\langle\overline{\boldsymbol{u}}\rangle_s$ is already known and non-zero only for wake field fluctuations, which have $\omega = 0$. The interaction between the turbulent fluctuations and spatial variation of the roughness geometry, $\hat{\boldsymbol{d}}_{\boldsymbol{k}}$, is not known *a priori* but is assumed to be small, such that the forcing in the roughness sublayer is dominated by the wall boundary condition via the drag model, and the weights on the resolvent forcing modes are determined using

$$\chi_{\boldsymbol{k},j} \triangleq \left\langle\phi_{\boldsymbol{k},j}, -\hat{D}_{\boldsymbol{k}}\langle\overline{\boldsymbol{u}}\rangle_s\right\rangle. \tag{2.9}$$

We consider first the ability of RAVP to capture an efficient representation of amplified wake field modes, for which $\omega = 0$ by construction and thus the resolvent in (2.7) could be modified accordingly. The resolvent operators are computed on an $N_y = 200$ point Chebyshev grid defined on $y_{cheb} \in [-1, 1]$ and we calculate and use 25 of the leading symmetric resolvent modes for modelling. Since resolvent modes with support restricted to the near wall region appear in symmetric and antisymmetric pairs, the symmetric modes are sufficient to describe the effect of roughness that is mirrored on the top and bottom walls. Comparison of the streamwise and wall-normal velocity components of a representative wake field mode from the DNS with the leading (first) resolvent mode obtained from RAVP using the plane-averaged mean field (figures 2*b* and 2*c*) shows associated improvement in agreement between the location of the peak amplitude for RAVP modes and data relative to classical (non-drag-modified) resolvent analysis using either the relevant smooth or rough wall means. These panels effectively isolate the influence of the drag modified operator (i.e. (2.7)); the influence of the forcing model in (2.9) is additionally considered when integrated across scales in figure 3. Further, the normalized projection of the DNS wake field data onto the first symmetric RAVP response mode is high in the region where the TKE of the wake field is significant, shown in figure 2(*d*) (for this roughness, confined to the lowest values of streamwise and spanwise wavenumbers).

Turning to the nonlinear forcing, the associated spectrum of the nonlinear weights on the first resolvent modes, $\chi_{\boldsymbol{k},1}$ (2.8), is shown in figure 2(*e*). The most active modes lie in a similar wavenumber range to the response, with differences due to the relative

https://doi.org/10.1017/jfm.2026.12017 Published online by Cambridge University Press

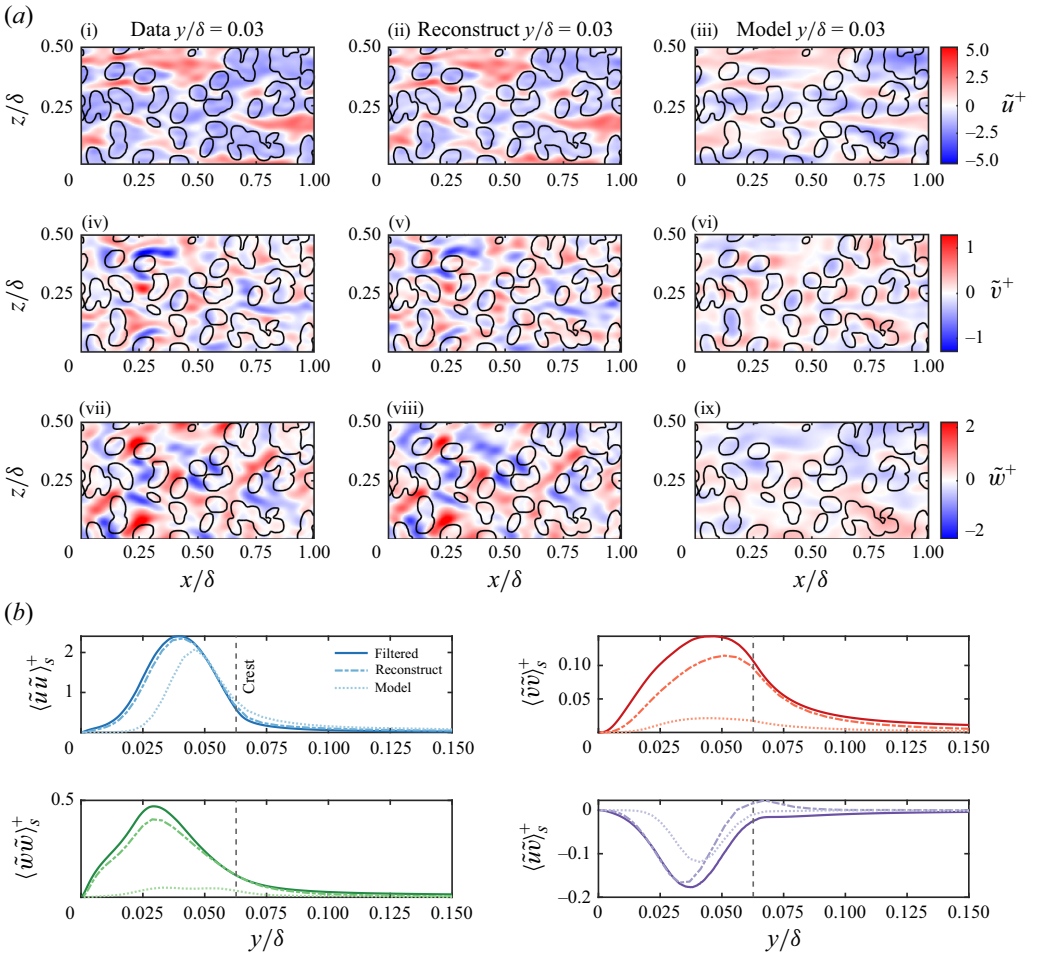


Figure 3. (*a*) Comparison of the wake field from (i,iv,vii) the data, (ii,v,viii) the model reconstruction and (iii, vi,ix) the compressed model. From (i–iii) to (vii–ix), streamwise, wall-normal and spanwise velocity components at $y/\delta = 0.03$ are shown. Black lines show the location of the edges of the (full) roughness geometry in this plane. (*b*) Wall normal variation of the dispersive stresses from data, model reconstruction and compressed model.

gains of each mode, which is encapsulated in the variation of $\sigma_{\boldsymbol{k},1}$ with $\boldsymbol{k}$. We further compress the RAVP representation of the roughness following the insight of Mejia-Alvarez & Christensen (2010) by low-pass filtering the Fourier representation of the roughness geometry from a total of $N_{k_x} \times N_{k_z} = 512 \times 256$ wavenumbers, to a subset consisting of the lowest 64×128 wavenumbers (justified for this roughness with reference to figure 2*d*). The associated distribution of weights computed from this reduced set of wavenumbers and the linearized forcing model of (2.9) is given in figure 2(*f*).

The impact of the filtering is not negligible in terms of comparison of the compressed RAVP model with the DNS wake field or the full RAVP reconstruction, which is able to capture the velocity variations with reasonable fidelity (figure 3*a*). Similarly, while the normal dispersive stresses in figure 3(*b*) are not very well captured by the compressed RAVP (wall-normal in particular), the dispersive shear-stress profile is reasonable, suggesting that key correlations between velocity components are retained. The wake fields underscore the origin of the latter point. While compressed RAVP preferentially weighs

https://doi.org/10.1017/jfm.2026.12017 Published online by Cambridge University Press

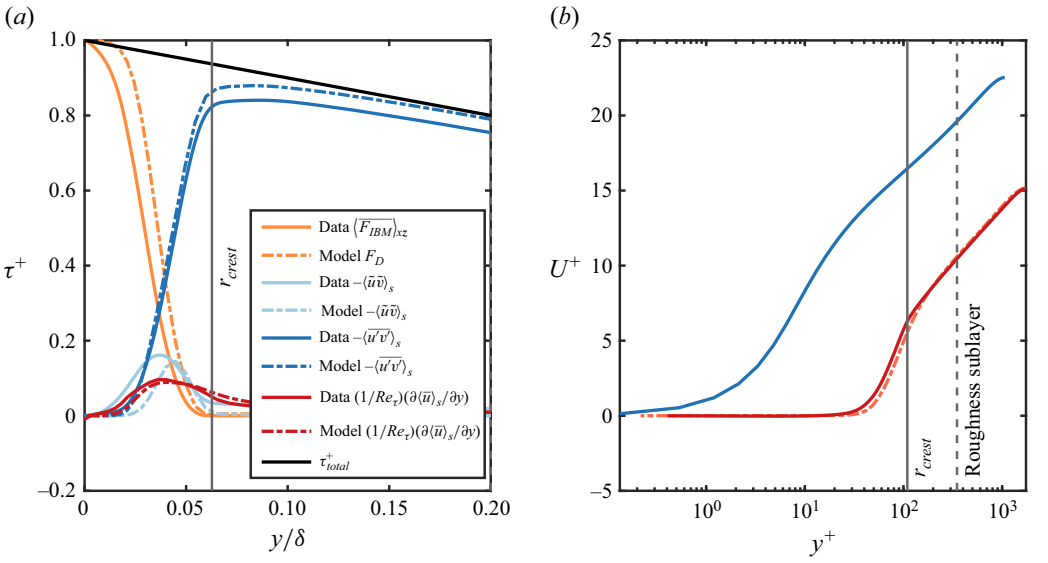


Figure 4. (*a*) The iterative mean flow model converges the components of the mean flow balance towards the true (DNS data) variations. (*b*) After $N_{eval} = 162$ iterations and initialization with the smooth wall profile (shown in blue), the model mean flow profile (dashed red line) has converged well to the true rough wall profile (solid red line).

large wavelength fluctuations in the roughness sublayer, the phase relationships between velocity components across all scales are such that the dispersive shear-stress is reasonably preserved and a substantially simplified model for the response of the flow to the varying roughness geometry can be obtained.

3. Iteration for the mean flow and wake field: prediction of turbulent flow response

The dispersive stresses obtained using compressed RAVP for a given roughness geometry and an estimate of the mean velocity profile are now employed in an iterative loop, which we deem RAVP-M, to determine the true mean-velocity profile, figure 1(*b*). The mean streamwise momentum equation for a rough wall requires consideration of the drag force due to the roughness, F_D, the rough wall stochastic stress as well as the dispersive stress,

$$\frac{\mathrm{d}}{\mathrm{d}y}\left[\frac{1}{Re_\tau}\frac{\mathrm{d}\langle\overline{u}\rangle_s}{\mathrm{d}y} - \langle\overline{u'v'}\rangle_s - \langle\tilde{u}\tilde{v}\rangle_s\right] + F_D = -1, \tag{3.1}$$

as shown in figure 4(*a*). The drag force F_D, which represents the plane-average of viscous and pressure forces on the roughness elements, can be modelled based on the mean momentum forcing term from RAVP,

$$F_D(\langle\overline{u}\rangle_s, \varphi) = -\langle D\rangle_{xz}\,\langle\overline{u}\rangle_s, \tag{3.2}$$

where we use the scalar D_{max} of (2.6). As noted above, this term can be cheaply evaluated given only the mean velocity profile.

We use a modified eddy viscosity profile, $\nu_{T_r}(y)$, to model the superficial average of the stochastic Reynolds stress, $\langle\overline{u'v'}\rangle_s$. Here $\nu_{T_r}(y)$ is monotonically attenuated from the equivalent smooth wall value, $\nu_T(y)$ (obtained using the Cess model with parameters $\kappa = 0.426$ and $B = 25.4$ (Del Álamo & Jiménez 2009)), at the top of the roughness sublayer to

https://doi.org/10.1017/jfm.2026.12017 Published online by Cambridge University Press

zero at $y = 0$ using a piecewise continuous function, $\zeta(F_D)$, such that

$$\nu_{T_r} = (1 - \zeta(F_D))\nu_T, \qquad \zeta(F_D) = g(y;\, y_0, \gamma) = \frac{1}{1 + \left(\dfrac{y - y_0}{C\gamma}\right)^2}. \tag{3.3}$$

A Cauchy function constructed to peak at the walls and provide wall-normal support in agreement with the wall-normal extent of the drag force F_D is selected for $\zeta(F_D)$. Here y_0 denotes the peak location, and γ is the scale parameter which specifies the half-width at half-maximum of the normalized Cauchy function. The values of C and γ together define the attenuation of the eddy viscosity expected in the presence of roughness. A (constant) value of $C = 3.04$ is found to be suitable for describing the behaviour of the rough wall eddy viscosity (figure 4*a*); this is analogous to the depth of the roughness sublayer. At a given iteration i, γ is defined based on the best fit to the shape of F_D. While it would be possible to use different functions, $\hat{\zeta}(F_D)$, for the top and bottom of the channel, here the functional form remains the same since each wall has identical roughness statistics.

The solution for the mean flow is now iterative, as laid out in figure 1(*b*), with inputs of the surface roughness geometry, $k(x, z)$, and an initial guess for the inner-scaled mean flow profile $\langle\overline{u}\rangle_s^{(i)}$ at the desired bulk Reynolds number $Re_b^{desired}$. RAVP gives predictions for the drag force and dispersive stress, then the MMB is solved to give a new inner-scaled mean profile, $\langle\overline{u}\rangle_s^{(i+1)}$. From this mean profile, $u_\tau^{(i+1)}$, a new $Re_b^{(i+1)}$ and a new $Re_\tau^{(i+1)}$, if needed, are computed using

$$u_\tau^{(i+1)} = \frac{1}{\int_0^1 \langle\overline{u}\rangle_s^{(i+1)}\,\mathrm{d}y};\; Re_b^{(i+1)} = \frac{Re_\tau^{(i)}}{u_\tau^{(i+1)}};$$
$$Re_\tau^{(i+1)} = Re_\tau^{(i)} + \left(Re_b^{(i+1)} - Re_b^{desired}\right) u_\tau^{(i+1)}. \tag{3.4}$$

The equations are discretized and solved using Chebyshev differentiation matrices (Weideman & Reddy 2000). The iteration is initialized using the smooth-wall mean profile for the Re_b of interest as a readily available initial guess for the velocity field and zero dispersive stress. Compressed RAVP for the dispersive stress is first evaluated at the second iteration to allow the mean profile shape to be somewhat corrected by the drag term and adjusted eddy viscosity during the first step, which leads to a better estimate for the dispersive stress, and then again every N_{update} iterations to reduce cost while still encoding the relationship between the mean flow profile and dispersive stress. Iteration through this loop continues until the resulting bulk Reynolds number matches the desired bulk Reynolds number to a chosen error, $|Re_b^{(i+1)} - Re_b^{desired}| < \epsilon\, Re_b^{desired}$ for a given choice of ϵ, a user selected error tolerance on the bulk Reynolds number. The resulting evolution of the values of Re_b, Re_τ and u_τ is plotted in figure 5(*a–c*). All these quantities converge monotonically towards the true values, where the discontinuities correspond to where the dispersive stress is updated, however, the stopping criterion is based on the error tolerance for the bulk Reynolds number for consistency with the conditions that are used as input to RAVP-M. Here ΔU^+ and k_s^+ are evaluated using the average deviation of the mean velocity from a log law with smooth wall constants $\kappa = 0.39$ and $B = 5$ over $y^+ \in [3Re_\tau^{0.5}, 0.15Re_\tau]$, and the fully rough relationship between them with $D_r = 7.9$, which is in the range observed for most rough wall surfaces:

$$k_s^+ = \exp\left[\kappa(\Delta U^+ - B + D_r)\right]. \tag{3.5}$$

https://doi.org/10.1017/jfm.2026.12017 Published online by Cambridge University Press

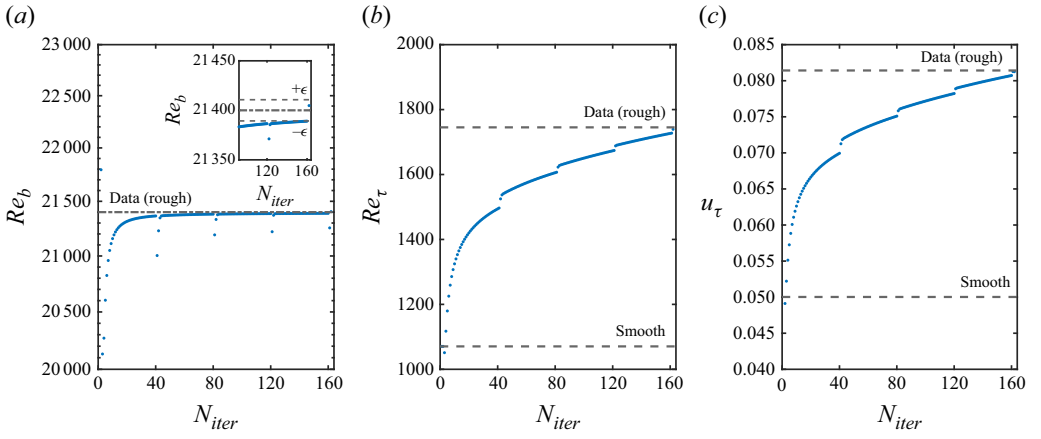


Figure 5. (*a*) The Re_b evolution with iteration number. The inset depicts the final convergence to within the ϵ bounds. (*b*) The Re_τ evolution with iteration number. (*c*) The u_τ evolution with iteration number.

We used iteration parameters $\epsilon = 0.0005$, $N_{update} = 40$ and $N_{eval} = 162$ to obtain the results in figure 4(*a,b*) in approximately 2 hours.

The modelled MMB terms closely approximate those from the DNS, with a slight underestimation of the mean flow gradient within the roughness geometry. The dispersive stress is underestimated because the model for the weights $\chi_{k,j}$ in (2.9) underestimates streamwise wake field fluctuations at $y/\delta < 0.05$, as illustrated earlier in figure 3(*b*). The drag force is slightly overestimated, which is characteristic of the RAVP analysis, while the stochastic stress agrees well with the data. Nonetheless, the RAVP-M rough wall mean velocity (figure 4*b*) agrees well with the DNS, with minor differences observed deep into the roughness, well below the roughness crest. The computed values of friction Reynolds number, ΔU^+ and k_s^+ are shown in table 1. Here Re_τ is recovered within 0.4 % accuracy, while the evaluations of Hama roughness factor and equivalent sandgrain roughness, which depend on the precise definitions employed to determine them, are also within 2 % of the DNS values.

4. Discussion

The RAVP of channel flow over roughness with a drag-normalized, Reynolds-decomposed treatment of the volume penalization term has been shown to lead to an effective transfer-function relationship between wall-roughness scales and the response of the turbulent fluctuations, as embodied in the dispersive stress $\langle \tilde{u}\tilde{v} \rangle_s$. Exploiting the scale-dependent sensitivity of the flow response to compress the RAVP model and then embedding it in the MMB for rough walls alongside the mean drag from the volume penalization and a roughness-discounting for the eddy viscosity, RAVP-M provides a closed-loop, iterative method to determine the response of wall turbulence at a given bulk Reynolds number to specific, inhomogeneous roughness geometry, without the need for expensive, roughness resolving DNS. Such 'surface-specific' calculations are efficient due to their linear nature, the downsampling of the roughness geometry that was implemented to remove finescale features to which the flow is not sensitive and the parallelizable nature of the wavenumber-by-wavenumber calculation. Moreover, the approach provides an appealing framework by which to understand the response of turbulence to roughness in terms of the sensitivity of the flow to the length scales embedded in the surface. While more sophisticated modelling assumptions will be immediately apparent to the reader and will

https://doi.org/10.1017/jfm.2026.12017 Published online by Cambridge University Press

surely lead to better estimates of the full wake field, the present approach was sufficient to approximate the dispersive stress appearing in the rough-wall MMB and allow for converged estimates of the friction Reynolds number and equivalent sandgrain roughness that are in good agreement with the DNS results for randomly oriented, sandgrain-type ellipsoids at a medium Reynolds number. In ongoing work, we are advancing this conceptual framework by testing a range of Reynolds numbers, roughness types and flow configurations, including in spatial development and compound effects of roughness and pressure gradient, and considering its incorporation into LES wall models, consistent with the resolvent treatment we have proposed in Hantsis *et al.* (2026).

Funding. We gratefully acknowledge the Air Force Office of Scientific Research grant FA9550-21-1-0443.

Declaration of interests. The authors report no conflict of interest.

Data availability statement. The data that support the findings of this study are available on request.

References

Chan, M. 2024 Reduced order modeling of near-wall and roughness sublayer turbulence using resolvent analysis. PhD thesis, California Institute of Technology.

Chavarin, A. & Luhar, M. 2020 Resolvent analysis for turbulent channel flow with riblets. *AIAA J.* **58** (2), 589–599.

Del Álamo, J.C. & Jiménez, J. 2009 Estimation of turbulent convection velocities and corrections to Taylor's approximation. *J. Fluid Mech.* **640**, 5–26.

Flack, K. & Chung, D. 2022 Important parameters for a predictive model of k_s for zero pressure gradient flows. *AIAA J.* **60** (10), 5923–5931.

Flynn, Z., Bae, H.J. & Goza, A. 2024 Towards an immersed-boundary resolvent analysis framework for wall-bounded flows with various surface configurations. In *AIAA Aviation Forum and ASCEND 2024, AIAA Paper* 2024-3870. American Institute of Aeronautics and Astronautics.

Hantsis, Z., Chan, M.J., Hoang, N., McKeon, B.J. & Piomelli, U. 2026 Populating the wall layer, one eddy at a time: resolvent analysis for wall-modelled LES. *Intl J. Heat Fluid Flow* **117**, 110066.

Hantsis, Z. & Piomelli, U. 2020 Roughness effects on scalar transport. *Phys. Rev. Fluids* **5**, 114607.

McKeon, B.J. 2017 The engine behind (wall) turbulence: perspectives on scale interactions. *J. Fluid Mech.* **817**, P1.

Mejia-Alvarez, R. & Christensen, K.T. 2010 Low-order representations of irregular surface roughness and their impact on a turbulent boundary layer. *Phys. Fluids* **22** (1), 015106.

Meneveau, C., Hutchins, N. & Chung, D. 2024 The wind-shade roughness model for turbulent wall-bounded flows. *J. Fluid Mech.* **1001**, A3.

Weideman, J.A.C. & Reddy, S.C. 2000 A MATLAB differentiation matrix suite. *ACM Trans. Math. Softw. (TOMS)* **26** (4), 465–519.

https://doi.org/10.1017/jfm.2026.12017 Published online by Cambridge University Press